Inorganic Chemistry

Article

pubs.acs.org/IC

Ru[(bpy)$_2$(dppz)]$^{2+}$ and Rh[(bpy)$_2$(chrysi)]$^{3+}$ Targeting Double Strand DNA: The Shape of the Intercalating Ligand Tunes the Free Energy Landscape of Deintercalation

Duvan Franco,[†] Attilio V. Vargiu,[‡] and Alessandra Magistrato*[,§]

[†]International School for Advanced Studies (SISSA/ISAS), via Bonomea 265, 34136, Trieste, Italy

[‡]Dipartimento di Fisica, Università di Cagliari, s.p. Monserrato-Sestu km 0.700, I-09042 Monserrato, Italy

[§]CNR-IOM-DEMOCRITOS c/o International School for Advanced Studies (SISSA/ISAS), via Bonomea 265, 34136, Trieste, Italy

Supporting Information

ABSTRACT: Octahedral metal complexes can bind to double strand (ds) DNA either by intercalation or by insertion, this latter mechanism being observed in the case of mismatched base pairs (bps). In this work we modeled the process of deintercalation from the major groove for Δ-Ru[(bpy)$_2$(dppz)]$^{2+}$ (**1**) and Δ-Rh[(bpy)$_2$(chrysi)]$^{3+}$ (**2**), prototypical examples of metallo-intercalators and metallo-insertors, respectively. By using advanced sampling techniques, we show that the two complexes have comparable deintercalation barriers and that in both systems the main cost of deintercalation is due to disruption of $\pi-\pi$ stacking interactions between the intercalating moiety and the bps flanking the binding site. A striking difference between dppz and chrysi is found in their intercalation modes, being their longest axes, respectively, perpendicular and parallel to the P−P direction between opposite DNA strands. This leads the two ligands to deintercalate from the DNA through different mechanisms. Compound **1** goes through the formation of a metastable short-lived intermediate, with an overall free energy barrier of ∼14.5 kcal/mol, in line with experimental findings. Due to the length of the dppz intercalating moiety, an extended plateau appears in the free energy landscape at ∼3 kcal/mol above the most stable minimum. Compound **2** must cross a similar barrier (∼15.5 kcal/mol), but does not form intermediates along the deintercalation path, and the deintercalation profile is steeper than that found for **1**. Thus, the shape of the intercalating moiety affects the deintercalation mechanism of these inorganic molecules. This work is a first step to rationalize from a computational perspective the factors tuning the preferential binding mode of inorganic molecules (such as diagnostic probes, therapeutic agents, or regulators of DNA expression) to ds DNA.

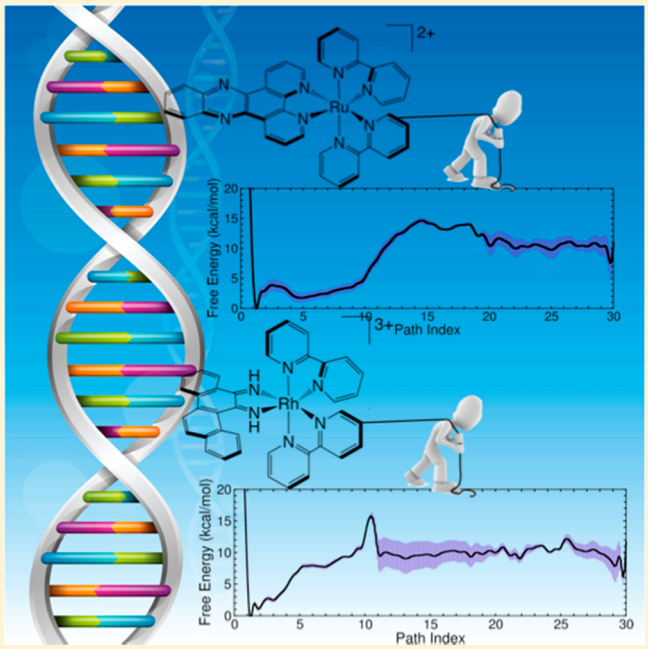

1. INTRODUCTION

The intercalation hypothesis, proposed 50 years ago and later confirmed by crystallographic studies, provided the first explanation for the binding of polyaromatic molecules to DNA.[1,2] These compounds, which include octahedral metal complexes bearing polyaromatic ligands,[3,4] can intercalate between adjacent standard base pairs (bps) of double strand (ds) DNA inducing small structural perturbations (Figure 1).[5] The first crystallographic structure of a Rh-based complex bound to DNA[2,3,6] showed the planar aromatic moiety intercalating from the DNA major groove (MG), and the bulky ancillary ligands of the complex snugly fitting to the MG walls.[7] These inorganic compounds can also bind from the minor groove (mG) at mismatched sites, expelling the mismatched bases and acting as their π-stacking replacement (Figure 1). This binding mode is usually referred to as insertion.[4,8−10]

An archetypal metallo-intercalator is Ru[(bpy)$_2$(dppz)]$^{2+}$ (bpy = 2,2′-bipiridine, dppz = dipyridophenazine) (**1**, Figure 2).[9] These kinds of Ru-based compounds have peculiar photophysical properties as their luminescence is switched on by the presence of DNA ("light-switch" effect).[11−14] In contrast, Rh[(bpy)$_2$(chrysi)]$^{3+}$ (chrysi = chysene-5,6-quinone-

Received: April 11, 2014
Published: July 23, 2014

   dx.doi.org/10.1021/ic5008523 | Inorg. Chem. 2014, 53, 7999−8008

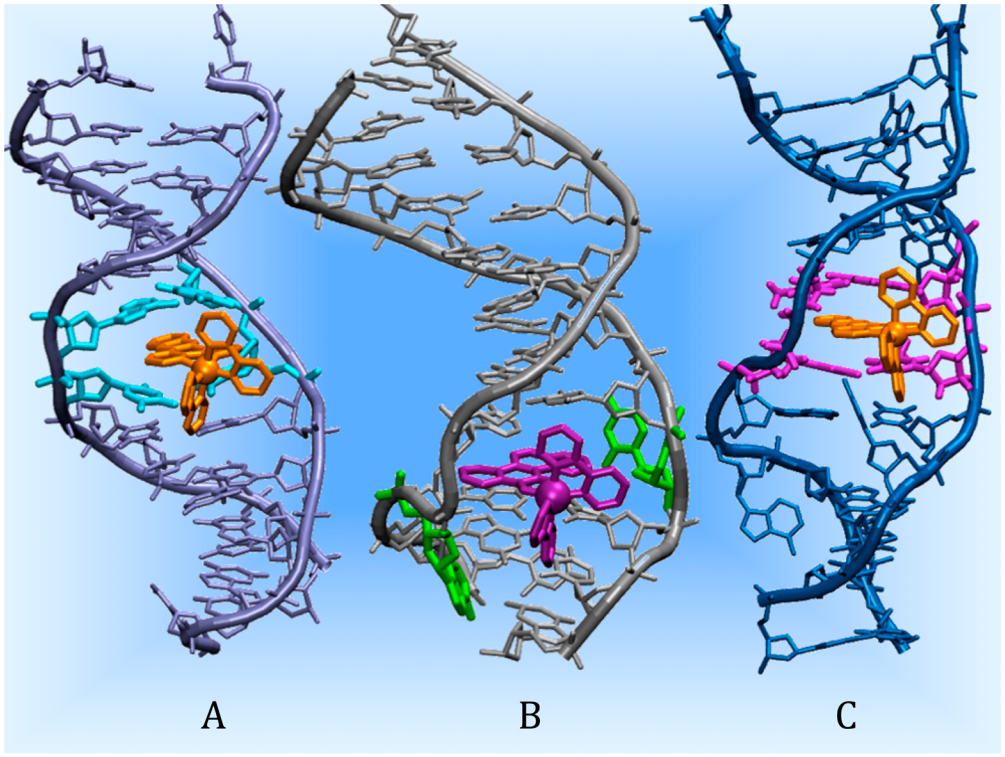

Figure 1. Intercalation of **1** from the MG of dsDNA (A); insertion of **2** into a mismatched bp (B); intercalation of **1** into DNA mG (C). A and B are representative equilibrated structures extracted from our simulations (the models were built from the X-ray structure of **2** intercalated and inserted into a DNA dodecamer (PDB Code: 2O1I), while C displays the X-ray structure of **1** intercalated from the mG (PDB Code: 4E1U). In order to simplify the image the two terminal molecules inserted in this sequence are not shown.

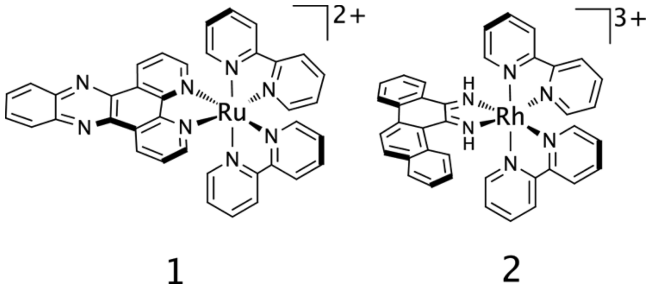

Figure 2. Chemical structures of the ruthenium and rhodium complexes studied in this work, Δ-$[Ru(bpy)_2(dppz)]^{2+}$ (**1**) and Δ-$[Rh(bpy)_2(chrysi)]^{3+}$ (**2**).

diimine) (**2**, Figure 2) is a prototypical metallo-insertor as it specifically binds to single mismatches, single base bulges, and abasic sites.[15−17] **2** is highly mismatch specific (it can target a mismatch over 2700 DNA bps), binding to 80% of mismatches in all possible DNA sequences.[4,6,15,18] Most importantly, this complex has been demonstrated to exert an antiproliferative effect in mismatch repair deficient cell lines *in vivo*.[17] In fact, light irradiation of Rh complexes determines a photocleavage of the DNA backbone, leading to cell death.[4]

Despite the preferential binding modes of **1** and **2** being likely different, both compounds can intercalate and insert to ds DNA.[6,11,19] For instance, it has been reported that **1** can also insert at a mismatched site from the mG,[18] while **2** has been observed to intercalate into the MG by X-ray studies.[6]

Experimental kinetic studies[13,20−24] showed that the binding of **1** to DNA is characterized by an entangled entropically driven multistep mechanism,[19,21−23] which involves the formation of partially intercalated states, as confirmed by X-ray and kinetic studies,[9,12,22,24] and of a groove-bound adduct.[12] The binding mechanism of compound **2** has not been a subject of mechanistic study due to the lack of luminescence, and it is therefore of particular interest for computational studies.

In this work we studied the deintercalation mechanism of **1** and **2** from the MG of dsDNA. This process is the first and rate-determining step[25−27] of a multistep dissociation mechanism and leads to a groove-bound state from which complete dissociation occurs. We performed force-field based well-tempered metadynamics simulations (WT-MTD)[28] using path collective variables (PCV).[29] The use of enhanced sampling methods within the framework of path variables has been successfully applied to several biological problems.[30−34] However, WT-MTD combined with PCV has been never used to study the mechanism of dissociation of a complex ligand from a flexible target such as DNA. Furthermore, to the best of our knowledge, this is the first computational study attempting to draw a molecular-level description of the recognition mechanism of DNA by octahedral transition metal complexes, which is still a matter of active debate.[9,18,35]

Our results confirm the striking difference between the intercalation modes of dppz (**1**) and chrysi (**2**), being their longest axes respectively perpendicular and parallel to the P−P direction between opposite DNA strands. The two complexes have comparable deintercalation barriers of ∼14.5 (**1**) and ∼15.5 (**2**) kcal/mol, mainly arising from the disruption of $\pi-\pi$ stacking interactions between the intercalating moiety and the bps flanking the binding site. Apart from this common feature, they deintercalate from the DNA through different mechanisms. Namely, the deintercalation of **1** occurs via formation of a metastable short-lived intermediate, which is consistent with experimental findings[20−22] and similar to the mechanism found

dx.doi.org/10.1021/ic5008523 | *Inorg. Chem.* 2014, 53, 7999−8008

for purely organic intercalators.[25,27] Due to the appreciable length of the dppz intercalating moiety, an extended plateau appears in the free energy landscape at ∼3−4 kcal/mol above the most stable minimum. Compound **2**, instead, does not form intermediates along the deintercalation path, and the free energy profile is steeper than that found for **1**. Thus, the shape of the intercalating moiety significantly affects the dissociation mechanism of these inorganic molecules.

This study, focusing on intercalation, constitutes a first step toward discriminating the factors affecting the preferential binding mode of **1** and **2** to dsDNA. Nonetheless, the comparison of our results with literature data on these and others classes of intercalators allows proposing a general picture of the factors modulating an effective intercalation binding mode. Our study points to structural aspects that may be tuned to enhance differences in the free energy profile of typical metallo-insertors and intercalators and could be of help in the design of new selective intercalating agents.

2. COMPUTATIONAL DETAILS

2.1. Model Systems. The noncovalent adducts between compounds **1**, **2**, and the oligonucleotide 5′-d[CGGAAATTCCCG]-3′ were built following the same procedure found in ref 36. Namely, we used as a template the crystal structure of Δ-$[Rh(bpy)_2(chrysi)]^{3+}$ (**2**) in a complex with the same oligonucleotide sequence reported above (PDB Code: 2O1I).[6] This structure contained two terminal and symmetric Δ-$[Rh(bpy)_2(chrysi)]^{3+}$ inserted into the mG and one molecule intercalated in the MG.[37] To build a model for intercalation of **1** into the crystallographic DNA dodecamer we removed the two compounds inserted into the mG, reestablishing the standard Watson−Crick configurations of the 4−21 and 9−16 base pairs by rotating them back from the extrahelical position and by replacing the A nucleobase at positions 4 and 16 with G. (Residues from the 5′ to 3′ end on the first strand are numbered from 1 to 12, while 5′ to 3′ residues on the second strand are numbered from 13 to 24.) To build the intercalation adduct for **1**, the bpy ligands, the metal, and the coordination bonds of the inserting ligand were superimposed with those of **2** in the crystal structure. The two molecules are intercalated between A6-T19 (Flk1) and T7-A18 (Flk2). We have studied here only the Δ-enantiomer, as it is the only stereoisomer for which the binding of both complexes to DNA has been determined crystallographically.[6,9] Moreover, the photophysical properties of Ru compounds are stereochemistry dependent, and this enantiomer has higher luminescence.[12,18]

2.2. Molecular Dynamics Simulations. The PARMBSC0[38] refinement of the parm99 force field[39] was used for the oligonucleotide moieties. The intercalators were parametrized as described in refs 36 and 40. In addition, we tested the dependence of our parametrization on the set of point charges employed via a force matching procedure.[41,42] Water molecules were described with the TIP3P potential.[43] Na^+ ions were added to achieve neutrality and modeled with the Aqvist potential.[44] The two systems, each including the inorganic molecule, the DNA dodecamer, explicit waters, and ions, count up to 23 000 and 24 000 atoms for **1**/DNA and **2**/DNA, respectively. Electrostatic interactions were evaluated with the particle mesh Ewald (PME) method.[32] A cutoff of 10 Å was used for the van der Waals (vdw) interactions and the real part of the electrostatic interactions. A time step of 1.5 fs was applied, and all bonds were restrained using the LINCS algorithm. Room-temperature (300 K) simulations were achieved by coupling the systems to a Nose−Hoover thermostat.[45] The starting structures for the generation of the initial path to run PCV-metadynamics simulations were taken from our previous study.[36] The DNA structural parameters and the hydration of the grooves are compared to those extracted from a previous MD simulation of a B-DNA oligonucleotide free of ligands.[36] All (plain and biased) molecular dynamics (MD) simulations were performed with GROMACS4.0.7.[46]

2.3. Metadynamics Simulations. The computational protocol employed to perform metadynamics simulations consisted of three steps: (i) building of an initial "guess" deintercalation pathway from DNA; (ii) optimization of the path starting from the initial guesses; and (iii) free energy calculations over the optimized path.

2.3.1. Generation of the Initial Guess Path for PCV-Metadynamics Simulations. The initial guess paths were generated by performing Steered Molecular Dynamics (SMD) simulations on the equilibrated system,[47] using as a collective variable (CV) the distance between the centers of mass of all heavy atoms belonging to the ligand and that of Flk1 and Flk2. For both complexes we performed an SMD run of 11.25 ns (in line with recent studies[33]) with a steering velocity of 1.34×10^{-6} Å/step, moving the complexes from the intercalated state up to a distance of 15 Å, which corresponds to full dissociation of the compounds from the DNA. The steering force constants were 0.060 and 0.084 kcal mol^{-1} $Å^{-2}$ for **1**/DNA (initial distance 6.1 Å) and **2**/DNA (initial distance 6.8 Å), respectively. (The force constants used to perform the SMD simulations were calculated by considering the fluctuations (standard deviation, STD) of the respective collective variable (distance between the centers of mass or S(R)), along a corresponding unbiased MD simulation with the relation: $\kappa = {}^1/_2(k_BT)/(\mathrm{STD}).^2$) A total of 30 frames, equally spaced in root-mean-square deviation (RMSD), were extracted from the SMD trajectories and used as initial guesses for the dissociation paths.

2.3.2. Optimization of the Initial Guess Paths Using SMD and PCV. We then applied an iterative protocol to optimize the generated guess paths using the Path Collective Variables.[29] PCV are a couple of variables, namely S(R) and Z(R) (eq 1 and 2, respectively), with R being the Mean Square Deviation (MSD), and λ being a tunable parameters, which represents the smoothness of the path. These variables are able to describe the transition between two different conformations. In the discrete implementation of PCV-metadynamics available in PLUMED 1.2 and used here they are defined as[48]

$$S(R) = \frac{\sum_{i=1}^{P} i e^{-\lambda(R-R(i))^2}}{\sum_{i=1}^{P} e^{-\lambda(R-R(i))^2}} \quad (1)$$

$$Z(R) = -\frac{1}{\lambda}\ln\left(\sum_{i=1}^{P} e^{-\lambda(R-R(i))^2}\right) \quad (2)$$

P is the number of frames; i.e. i is a discrete index and varies between 1 and 30, so that here S(1) represents the intercalated state, while S(30) represents the dissociated one. In practice, S(R) and Z(R) represent the intercept (motion along the optimized path S(i)) and the distance from S(i), respectively, of any microscopic configuration R. As specified in ref 29, Branduardi, D.; Gervasio, F. L.; Parrinello, M. *J Chem Phys* **2007**, 126, 054103, two conditions should be satisfied in order to produce the smooth behavior of S(R) and Z(R): (i) the frames chosen should be as equidistant as possible, and (ii) the parameter λ should be comparable to the inverse of the mean RMSD between consecutive frames.

Our iterative optimization process consisted of four consecutive SMD runs of 11.25 ns each, using the same CV of previous SMD runs but with a steering velocity of 2.67 S_{path}-units/ns and with spring constants of 2.3 kcal/mol for **2** and 1.2 kcal/mol for **1**. In all runs, a harmonic upper restraint of 5 kcal/(mol·Å)^8 was imposed on Z(R) at the value 0.2 $Å^2$. We considered the path optimized after four SMD runs, as no further improvement of the λ value was observed (Table S1 of the Supporting Information).

As a further test to check the convergence of λ we ran another SMD simulation doubling the steering velocity. This resulted in the same deintercalation path in terms of RMSD and total work spent to move the system along the path (Table S1).

To further assess the smoothness of the pseudo-optimized path, we plotted Z(R) versus S(R) for the four SMDs simulations performed for **1** and **2** (Figure S1 of the Supporting Information).[34] Despite the larger oscillations of Z(R) seen in **2** as compared to **1**, Figure S1 shows that for both systems most of the discontinuities present in the initial paths are removed in the optimized ones, at least until a value of S(R)

dx.doi.org/10.1021/ic5008523 | Inorg. Chem. 2014, 53, 7999−8008

~20. Thus, the path is fairly smooth up to this point in both cases (see also Results).

2.3.3. Well-Tempered Metadynamics Combined with PCV. Free energy estimations of the deintercalation barriers were obtained by performing well-tempered metadynamics (WT-MTD)[28,49,50] simulations combined with PCV[50] on the optimized path. We used 30 equidistant consecutive frames from the optimized paths, with λ set to 4.51 Å^{-2} for **1** and 3.06 Å^{-2} for **2**. For each inorganic complex these values were obtained after taking the trajectory of the last SMD simulation and by optimizing the mean interframe RMSD value (over the 30 frames) by a self-consistent procedure. This procedure was repeated for 10 cycles, until when the mean interframe RMSD did not change more than 5%. WT-MTD is an extension of the standard metadynamics in which the rate of bias potential deposition decreases along the simulation, thus directing all the microscopic variables toward the thermodynamic equilibrium. An extra tuning parameter (ΔT) is used to limit the exploration of free energy regions that are physically relevant, normally chosen according to the energy barrier of the process of interest. In our case the temperature was set to 300 K, while the tuning parameter to 4200 K.

Gaussians of height 0.12 kcal/mol were deposited every 0.75 ps on the subspace defined by S(R), while Z(R) was left unbiased, following a commonly applied computational protocol.[30,33,34] This setup allowed us to sample states out of the optimized path, while maintaining the system close to the selected (and optimized) frames. A good convergence on the value of the highest deintercalation barriers was reached after 120 ns for both systems, and up to Path Index (PI) ~20 in the case of **1** (Figure S2) and up to PI ~ 11 for **2**. This was confirmed by the fair conservation of representative structures of the transition states (TS) extracted from a cluster analysis of the trajectories around values of S(R) corresponding to the TS region (Figures S3–S5). Because of the above observations we can be confident about our results for **1** and **2** in the ranges PI ≈ 0–20 and PI ≈ 0–11, respectively. Despite the final part of the deintercalation process being, thus, poorly described by our setup, we obtained a reliable description of the key steps accompanying the deintercalation of **1** and **2** from DNA. The protocol used to gain an estimate of the error on the free energy profiles (FEP) is described in the Supporting Information.

2.4. Structural and Energetic Analyses. To identify structural and energy determinants associated with the deintercalation of **1** and **2**, we performed structural and energetic analyses on selected PIs. These are 1, 2, 5, 14, 16, 20, 26, and 29 in the case of **1** and 1, 7, 10, 13, 18, 22, and 29 in the case of **2** (Figures 3 and 6).

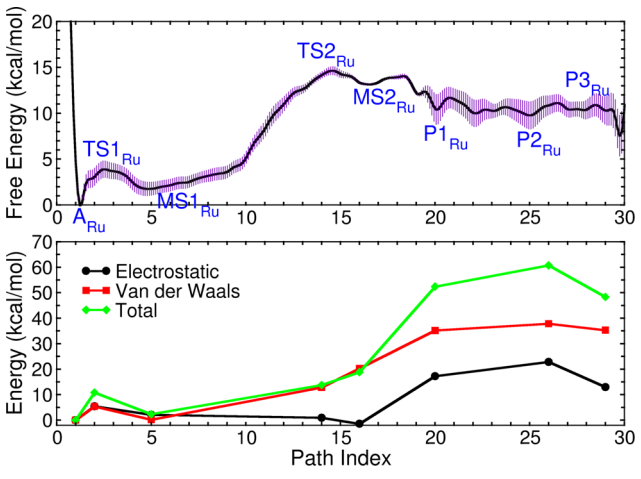

Figure 3. (Upper panel) Free energy profile associated with the deintercalation (kcal/mol) of **1** from the DNA MG. (Lower panel) Trend of the changes in the total, vdw, and electrostatic interaction energies between **1** and the oligonucleotide, in reference to the intercalated state and shown for selected PIs along the reaction path.

Structural parameters of the DNA (helix bending, buckle, opening, the rise, twist, roll, tilt, and propeller angles) were defined according to ref 51 and calculated with the program Curves+.[52] Radial distribution functions (RDF), root-mean-square deviations (RMSD), and structural clusters (Table S2) were calculated with the *ptraj* module of the AMBER tools.[39] The number of waters within the first and second shells of the mG and MG were also calculated with *ptraj*. For this purpose, we set the first and second hydration shell cutoffs by calculating the RDFs of N3@DA18, N3@DA6, O2@DT7, O2@DT19 for the mG; N6@DA6, N7@DA6@, O4@DT7, N6@DA18, N7@DA18, O4@DA19 for the MG; and the N atoms of the organic ligands. In this nomenclature the first letter and number refer to the atom type and number; the term @ indicates that this atom type belongs to the nucleobase mentioned after @. Interaction energies were calculated with the NAMD Energy plug-in version 1.4 in VMD 1.8.7, using a cutoff of 10 Å for the electrostatic interactions.[53] Stacking interaction energies between Flk1 and Flk2 were approximated by the vdw energies.

The free energy of hydration was calculated with the formula: $\Delta G_{hyd} = \Delta H_{hyd} - T\Delta S_{hyd}$, where $\Delta H_{hyd} = \Delta C_p \cdot (T - 295)$ kcal·mol^{-1}, and $T\Delta S_{hyd} = \Delta C_p \cdot \ln(T/386)$ kcal·mol^{-1}·K^{-1}, respectively.[54,55] The heat capacity ΔC_p was calculated as $0.32\Delta A_{np} - 0.14\Delta A_p$ kcal·mol^{-1}·K^{-1}, where A_p and A_{np} are the variations in the hydrophilic and hydrophobic surface areas, respectively,[54,55] calculated with the *g_sas* tool of the GROMACS4.0.7 package.[46]

3. RESULTS

3.1. Deintercalation Mechanism of Ru[(bpy)$_2$(dppz)]$^{2+}$. The free energy profile (Figure 3) shows that the deintercalation of **1** occurs with a first free energy barrier ($\Delta G_{diss}^{\#}$) of ~4 kcal/mol ($TS1_{Ru}$ in Figure 4), followed by the formation of a very shallow metastable intermediate ($MS1_{Ru}$), which is only about 2 kcal/mol higher in energy than the intercalated state and it is characterized by a lateral displacement of **1** toward the second strand of the DNA duplex (Figure 4). The shape of the dppz moiety allows this first part of the deintercalation process to occur along a pseudoplateau in the free energy profile (Figure 3), ~3 kcal/mol higher in free energy than the most stable minima. Then, a second transition state ($TS2_{Ru}$) is found, featuring a $\Delta G_{diss}^{\#}$ of ~13 kcal/mol (relative to $MS1_{Ru}$). After this point **1** first rearranges ($MS2_{Ru}$) and then laterally deintercalates, remaining in the vicinity of the MG ($P1_{Ru}$–$P3_{Ru}$, Figures S6 and S7). The remainder of the path is characterized by structural rearrangements of **1** within the MG walls, whose conformations resemble the mG-bound state observed also for organic intercalators[25−27] and postulated for metallo-intercalators.[12,24] Since $MS1_{Ru}$ is a short-lived metastable state, we can estimate an effective free energy barrier (from A_{Ru} to $TS2_{Ru}$) of ~14.5 kcal/mol associated with the deintercalation of **1**.

3.1.1. Structural Properties. We have analyzed in detail the DNA structural parameters at the selected PIs along the dissociation path (Figure S10), focusing on bps Flk1 and Flk2. Concerning the intrabp parameters, we see that both the buckle and propeller reflect an asymmetric deintercalation of **1** (Figure S10). Concerning the interbp parameters, the twist angle, small in the initial conformation (the DNA results to be undertwisted upon intercalation), decreases at $TS1_{Ru}$ and then increases again (approaching the value of free DNA) as far as the deintercalation proceeds (Figure 5). As expected, the rise shows a smooth and progressive decrease of its value along the deintercalation path until it reaches the typical value of canonical B-DNA (Figure 5), indicating the recovery of a typical bp–bp stacking conformation. This is true also for the roll, which has a value close to zero at the beginning of the

dx.doi.org/10.1021/ic5008523 | Inorg. Chem. 2014, 53, 7999–8008

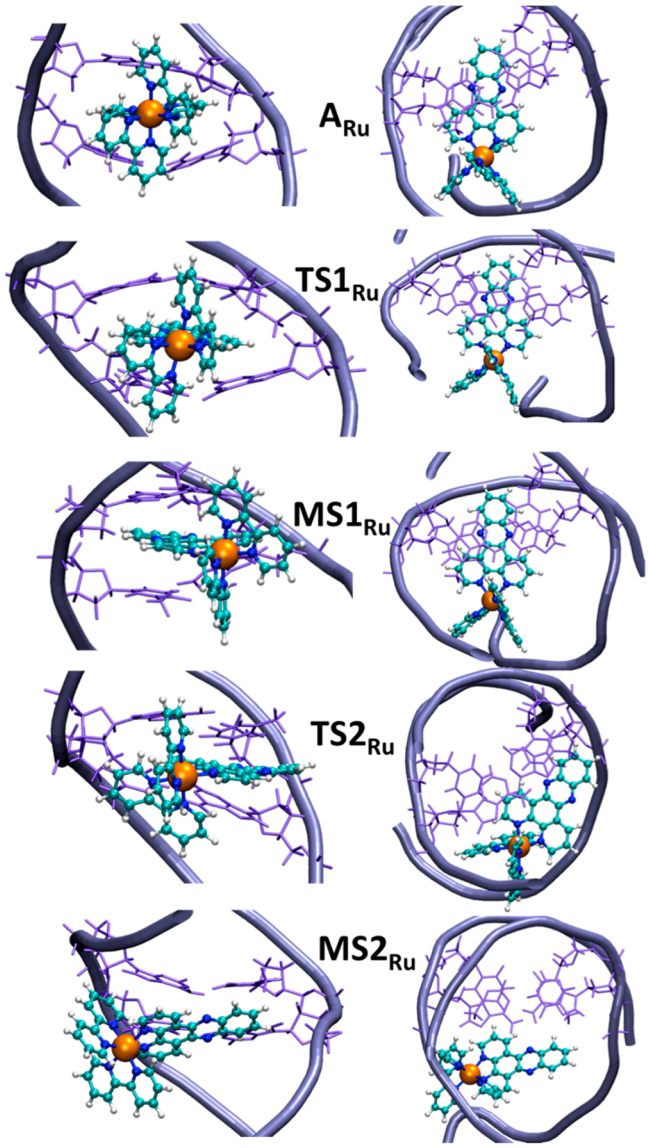

Figure 4. Side and top view of selected structures along the initial part of the deintercalation path of **1**. Each structure represents the most populated cluster of the trajectory corresponding to the selected PI (Table S2). The base pairs flanking the intercalation site (A6-T19 (Flk1) and T7-A18 (Flk2)) are represented in violet licorice. Ru is depicted as an orange vdw sphere, **1** is depicted in ball and sticks and colored by atom name.

path, consistently with opening of the bps toward the MG, and it almost progressively decreases along the deintercalation path until $P1_{Ru}$, from where it starts recovering the values typical of free DNA.

The local conformational changes depicted above reflect on global parameters such as bending and MG width (Figures 5 and S11).[56,57] In particular, the changes in roll, rise, and twist from A_{Ru} to $TS2_{Ru}$ induce an increase of the overall DNA axis bend from 30° to 70° that decreases then to 40° at $P3_{Ru}$ (Figure 5). The MG width, clearly larger than the typical B-DNA value upon intercalation, increases further at $TS1_{Ru}$, at both Flk1 and Flk2. Then, there is a progressive and smooth decrease along the path, with a small bump at $TS2_{Ru}$ for Flk2 (Figure S11).

3.1.2. Hydration Properties. We investigated the hydration properties of the major and minor groove during the

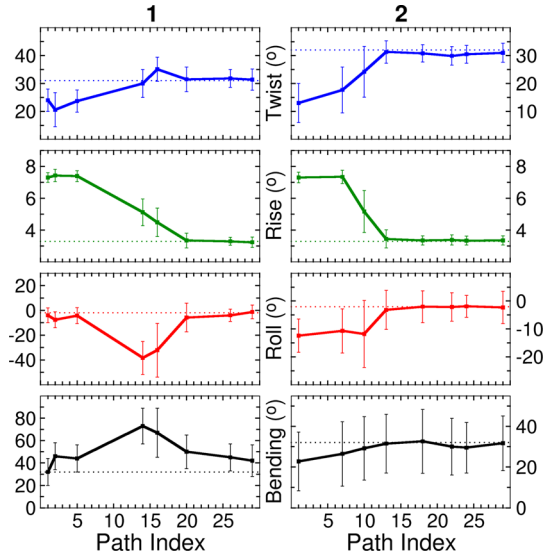

Figure 5. Trend of the interbp and global DNA parameters vs deintercalation path for **1** (left) and **2** (right) at Flk1/Flk2. Twist (°), rise (Å), roll (deg), and overall axis bending (deg) are reported. Values of free DNA, taken from ref 36, are reported as dotted lines.

deintercalation of **1**, considering both the first and second hydration shells around selected atoms (see Computational Details). A recent study has pointed out the importance of a conserved hydration network of water molecules in the binding of small molecules to the DNA mG.[58] However, in **1**/DNA we see that the hydration of both the mG and MG is poorly affected by the deintercalation of **1**, while, as expected, a significant change is observed in the hydration of **1** (Table S3).

3.1.3. Analysis of the Interaction Energies. We calculated the change in the nonbonded interaction energies between **1** and Flk1−Flk2 along the deintercalation path referred to as $\Delta E_{1/Flks}$. These data do not include any implicit screening by the solvent, so they are only meant to give an estimate of the main interactions playing a role in the process. As expected in the case of deintercalation, the largest changes are seen in the vdw term (Figure 3 and Table S4). $\Delta E_{1/Flks}$ increases by ∼11 kcal/mol at $TS1_{Ru}$ with respect to A_{Ru}; at $MS1_{Ru}$ it recovers a value similar to that in A_{Ru}, while at $TS2_{Ru}$ and $MS2_{Ru}$ there are losses of interaction by ∼14 and ∼19 kcal/mol, respectively, due to a striking decrease in the vdw interaction term. Consistently, there is a strengthening of the $\pi-\pi$ stacking energy between the Flk1 and Flk2 at the two TSs (by ∼4 and ∼8 kcal/mol, respectively; see Table 1), which partly compensates for the loss of vdw interaction energy between the intercalating moiety dppz and Flks at $TS2_{Ru}$ (Table 1). In the remainder of the path a progressive loss of the interaction energy occurs, with the MG-bound adducts ($P1_{Ru}$−$P3_{Ru}$) stabilized mainly by the electrostatic interactions with the DNA (Table S4).

In order to estimate the role of the solvent in the dissociation of metallo-intercalators, we also calculated ΔG_{hyd} according to refs 54 and 55 at selected PIs (Table 2). Despite the large standard deviations, a clear trend can be seen. As expected, ΔG_{hyd} increases progressively from the intercalated to the MG-bound states. As can be seen by comparing ΔH_{hyd} to $T\Delta S_{hyd}$, deintercalation is entropically driven, consistently with experimental data,[59] and with the data on the dissociation of mG binders.[54,55] The highly qualitative nature of these energies prevents performing additional interesting analyses such as the

dx.doi.org/10.1021/ic5008523 | Inorg. Chem. 2014, 53, 7999−8008

Table 1. Stacking Energies between Flk1 and Flk2 (kcal/mol) at the Selected PIs of the Dissociation Path for 1 and 2, Respectively[a]

1/DNA			2/DNA		
Path Index		vdw	Path Index		vdw
PI1	A_{Ru}	−3.4 (3.4)	PI1	A_{Rh}	−1.7 (0.2)
PI2	$TS1_{Ru}$	−4.8 (5.1)	PI7	$MS1_{Rh}$	−2.3 (0.6)
PI5	$MS1_{Ru}$	−4.1 (4.2)	PI10	$TS1_{Rh}$	−14.4 (4.2)
PI14	$TS2_{Ru}$	−7.9 (2.8)	PI13	$P1_{Rh}$	−17.6 (2.4)
PI16	MS2	−12.1 (4.3)	PI18	P2	−17.5 (2.6)
PI20	$P1_{Ru}$	−17.7 (2.4)	PI22	$P3_{Rh}$	−17.9 (2.6)
PI26	$P2_{Ru}$	−17.9 (2.7)	PI29	$P4_{Rh}$	−14.6 (3.8)
PI29	$P3_{Ru}$	−17.5 (3.5)			

[a]Standard deviations are reported in parentheses.

Table 2. Hydration Enthalpies (kcal/mol), Free Energies (kcal/mol), and Entropies (time, T) kcal/mol/K Calculated for Each Selected Points for Flk1, Flk2, and the Complex with Respect to the Dissociated States for 1 and 2 in (a) and (b), Respectively[a]

Path index		ΔH_{hyd}	$T\Delta S_{hyd}$	ΔG_{hyd}
PI1	A_{Ru}	−0.35 (0.17)	5.35 (0.01)	−5.7 (5.7)
PI2	$TS1_{Ru}$	−0.31 (0.18)	4.73 (0.01)	−5.0 (5.0)
PI5	$MS1_{Ru}$	−0.32 (0.16)	4.80 (0.01)	−5.1 (5.1)
PI14	$TS2_{Ru}$	−0.26 (0.17)	3.90 (0.01)	−4.1 (4.1)
PI16	$MS2_{Ru}$	−0.18 (0.15)	2.79 (0.01)	−3.0 (3.0)
PI20	$P1_{Ru}$	−0.16 (0.14)	2.37 (0.01)	−2.5 (2.5)
PI26	$P2_{Ru}$	−0.15 (0.13)	2.33 (0.01)	−2.5 (2.5)
PI29	$P3_{Ru}$	−0.15 (0.14)	2.24 (0.01)	−2.4 (2.4)

(a)

Path index		ΔH_{hyd}	$T\Delta S_{hyd}$	ΔG_{hyd}
PI1	A_{Rh}	−0.09 (0.13)	1.44 (0.01)	−1.5 (0.1)
PI7	$MS1_{Rh}$	−0.09 (0.13)	1.43 (0.01)	−1.5 (0.1)
PI10	$TS1_{Rh}$	−0.34 (0.14)	5.21 (0.01)	−5.6 (0.1)
PI13	$P1_{Rh}$	0.03 (0.15)	−0.52 (0.01)	0.6 (0.2)
PI18	$P2_{Rh}$	0.02 (0.13)	−0.35 (0.01)	0.4 (0.1)
PI22	$P3_{Rh}$	0.03 (0.15)	−0.50 (0.01)	0.5 (0.2)
PI29	$P4_{Rh}$	0.03 (0.14)	−0.49 (0.01)	0.5 (0.1)

(b)

[a]Standard deviations are reported in parentheses.

presence of the enthalpy−entropy compensation phenomena reported in the binding of some ligands to DNA.[60,61]

3.2. Deintercalation Mechanism of $Rh(bpy)_2(chrysi)^{3+}$.

The deintercalation of **2** occurs without the formation of any metastable intermediate (Figure 6). We report in the graph $MS1_{Rh}$, although it is not a metastable state, as no barrier is associated with the backward movement of **2** toward the intercalated state. The deintercalation of **2** occurs with a $\Delta G_{diss}^{\#}$ of ∼15.5 kcal/mol and after $TS1_{Rh}$ the complex is no longer intercalated inside DNA (Figure 7), but it explores several configurations interacting with the MG walls (Figures S12 and S13). Since the convergence of the free energy surface after $TS1_{Rh}$ is poor, the analyses performed on this part of the deintercalation path are largely qualitative and, thus, will not be discussed in detail.

3.2.1. Structural Properties. Concerning the changes in the structural parameters of DNA, we observed that the buckle angles have opposite values on the two Flks, but they assume the typical value of B-DNA on both strands at $TS1_{Rh}$, i.e. the main transition state (Figure S14). This feature was already observed for **1**/DNA (Figure S10). In both Flks the propeller angles have a larger value than in the case of B-DNA, although

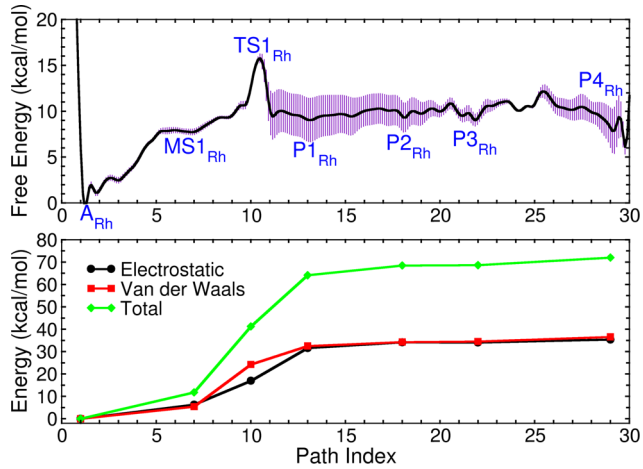

Figure 6. (Upper panel) Free energy profile associated with the deintercalation (kcal/mol) of **2** from the DNA MG. (Lower panel) Trend of the changes in the total, vdw, and electrostatic interaction energies between **2** and the oligonucleotide, in reference to the intercalated state and shown for selected PIs along the reaction path.

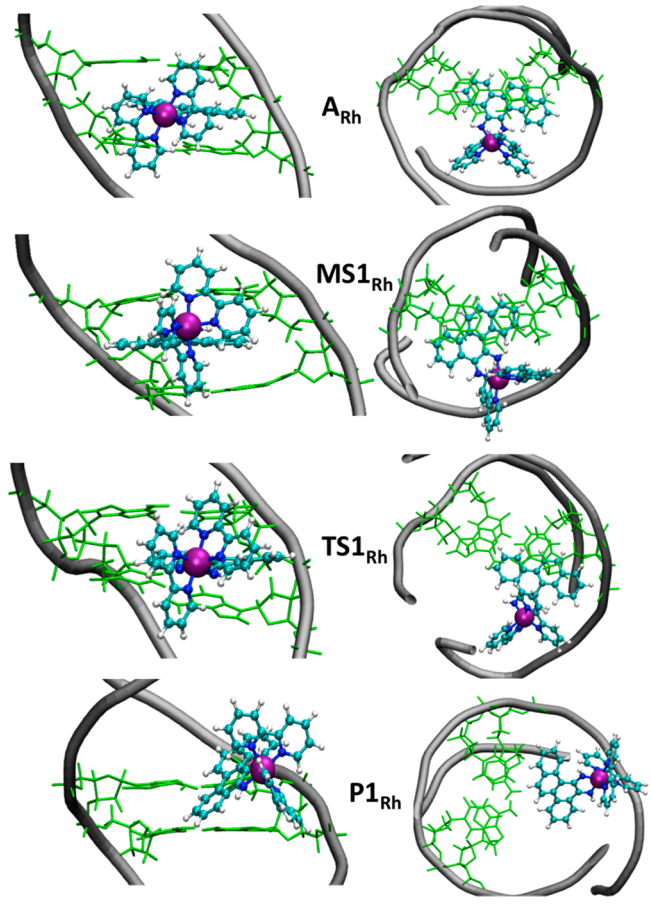

Figure 7. Side and top view of selected structures along the initial part of the deintercalation path of compound **2**. Each structure represents the most populated cluster of the trajectory corresponding to the selected PI (Table S2). The bps flanking the intercalation site (A6-T19 (Flk1) and T7-A18 (Flk2)) are represented as violet licorice. Rh is depicted as a purple vdw sphere, and **2** is depicted in ball and sticks form and colored by atom name.

dx.doi.org/10.1021/ic5008523 | Inorg. Chem. 2014, 53, 7999−8008

this value is remarkably different for the two Flks (Figure S14) up to $TS1_{Rh}$. Again, this behavior is shared with **1**/DNA, although the changes observed for the buckle and propeller angles are smaller than in the case of **1**/DNA.

Also the profiles of the interbp parameters roll, rise, and twist are overall similar to those found in **1**, and all these parameters return toward standard B-DNA values at/or just after the $TS1_{Rh}$ (Figure 5). However, compared to **1**, **2** induces a larger unwinding and a more prominent negative roll in the DNA[36] (Figure 5). An opposite trend is seen, instead, when comparing the overall axis bend along the deintercalation paths of **1** and **2**. In fact, in **2**/DNA the bending of the duplex increases smoothly during deintercalation, with a maximum variation of less than 10°, in contrast to **1** where a sudden increase of the overall axis bend up to 40° occurred at the two transitions states. The same difference is seen in the behavior of the MG width, which is larger in **2**/DNA than in **1**/DNA in the respective intercalated states, and for **2** it decreases more smoothly to the value typical of B-DNA (Figure S11).

3.2.2. Hydration Properties. The analysis of the hydration reveals that in **2**/DNA the mG undergoes small hydration changes (similar to those found in **1**/DNA), while, in contrast with **1**/DNA, the MG re-establish interaction with a significant number of water molecules upon detachment of the ligand (Table S3). The rehydration begins at $TS1_{Rh}$ (Figure S5), and this might be related to the difficulties in having a converged free energy profile after this point.

3.2.3. Analysis of the Interactions. The difference in the deintercalation modes of **1** and **2** is reflected also in the profiles of the interaction energy with DNA. Indeed, in contrast with **1**/DNA (Figure 3) a striking decrease of the vdw interaction energies takes place already at $TS1_{Rh}$ ($\Delta E_{2/Flks}^{\#}$ = 23 kcal/mol), and it continues progressively up to the MG-bound states (Figure 6).

As for **1**, $\Delta G_{diss}^{\#}$ is again partially ascribable to the breaking of the **2**/Flks vdw interactions (Table S4). However, in this case electrostatic interactions play a role comparable to that of the vdw energies, as Rh bears a larger fractional positive charge than Ru.

In contrast to what is observed in **1**/DNA, the deintercalation of **2** is characterized by a small ΔG_{hyd} (Table 2). However, there is a peak of −5.6 kcal/mol at $TS1_{Rh}$, rationalized in terms of the higher number of waters around the inorganic molecule (Table S3 and Figure S5). Thus, in terms of desolvation cost, deintercalation of **2** from DNA appears to be slightly favored, whereas its dissociation from the MG-bound states is slightly disfavored. This suggests that the major groove bound state may be more favorable for **2** rather than for **1**.

4. DISCUSSION AND CONCLUSIONS

In this section we first provide a brief summary of literature data about the intercalation of polyaromatic molecules into DNA oligonucleotides, which has been the subject of experimental[20,21] and theoretical[25−27,62,69] studies. Then, we compare and interpret our findings within this general framework with the aim of finding a general principle at the basis of the intercalation mechanism even between different classes of intercalating agents.

Kinetic studies suggested that intercalation of polyaromatic molecules occurs in at least three steps:[20,21] (i) a fast binding of the molecule to the DNA walls; (ii) an undefined state; and (iii) intercalation. The second state has been interpreted as a conformational readjustment of the drug and/or of the DNA binding site, or as the binding of the molecule to a different site.[21]

This picture has been supported by extensive computational studies on the intercalation/dissociation of daunomycin[25,62] to/from the mG of dsDNA. In refs 25 and 62 it was shown that intercalation of daunomycin occurs via an mG-bound intermediate, which is reached from the intercalated state after overcrossing a deintercalation barrier $\Delta G^{\#}$ of ∼9 (0.15 M NaCl aqueous solution)[62] or 13 (counterions only)[25] kcal/mol. This state features a binding free energy of ∼10 (0.15 M NaCl)[62] or 12 (counterions only)[25] kcal/mol.

Concerning metallo-intercalatators, kinetics studies carried out on $Ru[(phen)_2dppz]^{2+}$ (phen = phenantroline) revealed that its binding to ds DNA is entropically driven (ΔH_{bind} = +0.3 kcal/mol, $T\Delta S_{bind}$ = −11.1 kcal/mol).[59] Moreover, using stopped flow and spectrophotometric experiments, Biver et al. observed two binding regimes depending on the ratio concentration between the inorganic complex and the DNA.[24] While in the presence of a large excess of substrate there is a majority of an initially groove-bound state, a small excess of substrate shifts the equilibrium toward intercalation.[63] As suggested by previous theoretical studies the mechanisms of intercalation and deintercalation of daunomycin from ds DNA are similar, and these studies reveal that both intercalation/deintercalation processes include multiple steps.[62]

The authors of ref 24 also measured a kinetic constant k_d = 9.5 × 10^3 s^{-1} for the dissociation of $Ru[(phen)_2dppz]^{2+}$, consistent with a $\Delta G^{exp}{}_{diss}{}^{\#} \approx$ 12 kcal/mol. This barrier is smaller than that measured for planar metallo-intercalators, such as ZnNeotrien (2,5,8,11-tetraaza[12]-[12](2,9)[1,10]-phenantrolinophane) (k_d = 98 s^{-1}, which corresponds to $\Delta G^{exp}{}_{diss}{}^{\#} \approx$ 14.7 kcal/mol),[23] for which deintercalation has been observed to occur in one step, followed by the formation of a groove-bound state.[23] The difference between the dissociation free energy barriers of octahedral and planar inorganic complexes was experimentally ascribed to the existence of a partially intercalated intermediate occurring only for the octahedral compound.[59] Consistently with this interpretation, the presence of "side-on" and "head-on" intercalation states was also postulated on the basis of subtle solvatochromic differences in the mode of interaction of $Os[(phen)_2dppz]^{2+}$ and $Ru[(phen)_2dppz]^{2+}$ with DNA.[59,63,64] These two intercalated states were also confirmed by NMR and photophysical studies, and recently by X-ray crystallography.[6,9,18]

The findings of refs 24, 25, 62, and 63 match very well with our results for **1**. In fact, assuming that the intercalation path is exactly the reverse of the deintercalation one, as it occurs for daunomycin,[25,62] the intercalation of **1** appears to occur via binding to the major groove, followed by a first rearrangement, leading to a not fully intercalated state, from which a more stable intercalated state is reached through structural rearrangements of the DNA in a second and final step. It is worth noting that the dppz ligand of **1** intercalates in a similar way as the main body of daunomycin (see Figure S15 for a chemical sketch of the molecule). Furthermore, similarly to this compound and to $Os[(phen)_2dppz]^{2+}$ and $Ru[(phen)_2dppz]^{2+}$, also **1** is characterized by the presence of a metastable intercalated intermediate (Figure 3).[20,21,62] We speculate that such an additional (metastable) intercalated state could be more likely to occur for compounds having a "single file" polyaromatic moiety bound at one end to bulky groups (Figure

dx.doi.org/10.1021/ic5008523 | Inorg. Chem. 2014, 53, 7999−8008

S15), in a way that the intercalation must occur with the long axis of the polyaromatic moiety entering perpendicular to the P−P axis of opposite bases.

Concerning the kinetics of dissociation, there is an apparent difference of ∼2.5 kcal/mol between our calculated $\Delta G^{\#}_{diss}$ and that obtained experimentally for $Ru[(phen)_2dppz]^{2+}$. The reasons for the discrepancy could be many. At first, the inherent limitations of our approach can bias (at least in part) the results, as all the variables involved in the process are projected into a monodimensional path. For instance, the large changes in hydration observed for **2** (Table S3) could be related to the difficulty of obtaining a fully converged free energy profile within the time scale of our simulations. Although the selected variable S(R) seems to correlate quite well with the number of waters wetting the MG (Figure S16), the conformations found after/at the transition states ($TS2_{Ru}$ and $TS1_{Rh}$) likely represent states with unrelaxed waters around the site of binding. Nonetheless, the main findings discussed here should not be significantly flawed by these limitations. Indeed, during the first stage of deintercalation, when the steric restraints due to the DNA are limiting the conformational freedom of the inorganic compounds, the projection of the free energy along a monodimensional path should be fairly representative of the true process. Second, it has been shown that $Ru[(phen)_2dppz]^{2+}$ binds to DNA in different manners (MG and mG intercalation, and groove-bound state), whose relative population depends on the concentration of the metallo-intercalator, on the ionic strength, and on the temperature.[12] In particular, the dissociation constant extrapolated in ref 12, and corresponding to a barrier of ∼12 kcal/mol, refers to deintercalation from the less stable of two binding modes, which might well correspond to a partly intercalated state similar to, (but clearly more stable than), that found here for **1**. Third, the relative population of the "side-on" and "head-on" binding mode and their relative stabilities may be affected by the size of the ancillary ligands and by the ionic strength, with the population of the "side-on" adduct increasing at higher salt concentration.[12] For each of the aforementioned modes $\Delta G^{\#}_{diss}$ is highly sensitive to the ionic concentration. In fact, ΔG_{pol} has been estimated to be one-third of the binding free energy (∼ −3.7 kcal/mol),[59] which is fully consistent with the difference in the barriers found for daunomycin in refs 25 and 62. Moreover, since our simulations are not carried out at the same ionic strength of the experiments, a correction of this order of magnitude will result in a free energy barrier of ∼11 kcal/mol, in very good agreement with the value of ∼12 kcal/mol extracted from experiments.[12] The study of the influence of the ionic strength on the deintercalation free energy profile is certainly of interest, although it is beyond the scope of the present work.

Concerning the different mG and MG binding modes observed experimentally for $Ru[(phen)_2dppz]^{2+}$, our simulations cannot certainly exclude that for **1** intercalation may occur also from the mG side, as the two paths might be energetically comparable.[9,18] However, the intercalation of the Δ enantiomer of **1** inside the DNA mG observed by X-ray crystallography seems to be driven by extra-helical stacking due to the insertion of two additional compounds into the same oligonucleotide at sites adjacent to the intercalation one.[18] Indeed, the insertion of these compounds at the terminal parts of the same oligonucleotide determines a flipping of mismatched bases, which form π-stacking interactions with the ancillary ligands of the compound intercalated in the central part of the same oligonucleotide.[18] It has been suggested that the absence of mismatches could favor MG binding instead.[65] Consistently with this interpretation, "regular" intercalation from the mG has been observed only for $\Lambda-Ru[(phen)_2(dppz)]^{2+}$, whose phenantrolines can snugly pack onto the mG walls in a way that would not occur within the MG. Following Neidle,[65] we suggest that the small bpys present in **1** may shift the binding equilibrium toward the MG. In view of these considerations and of the fact that intercalation from the mG generally features a higher $\Delta G^{\#}_{bind}$,[26] our choice to focus here only on the path along the MG appears well justified.

As it clearly appears from recent structural studies,[66] several new puzzling findings are being added to the full picture of DNA molecular recognition by inorganic compounds, making its full understanding a much more challenging task than believed initially.[12,14,65−68] In this light, our work represents a first computational attempt toward understanding at the atomist level the factors influencing the preferential binding mode of octahedral inorganic molecules toward ds DNA. In particular, two important findings emerge, which could help the design of metallo-intercalators: (i) the shape of the intercalating ligand modulates the free energy profile of the intercalation/deintercalation processes; (ii) the charge and the shape of the intercalating ligand affect the amount of hydration/dehydration changes of the MG during the deintercalation/intercalation processes.

Clearly, the overall impact of these features also depends on the sequence of the DNA oligomer and on the groove (mG vs MG) where intercalation occurs. As a consequence, the short-lived intermediate observed here for **1** might be more stable in other DNA sequences or when intercalation occurs from the mG. Thus, our study could provide useful information on structural features to be addressed in order to modulate the free energy landscape of inorganic molecules binding to DNA.

Concerning **2**, since this compound can cleave the DNA upon irradiation, no photophysical studies are possible. However, the chrysi ligand is similar in shape to the intercalating moiety of ZnNeotrien, whose dissociation barrier from DNA, measured experimentally, matches very well the deintercalation free energy barrier calculated for **2**.

We remark that the free-energy barriers associated with the deintercalation of **1** and **2** are very similar. In principle, metadynamics simulations in which a statistically relevant number of intercalation/deintercalation events has been sampled can provide information also on the kinetics of the intercalation event. However, we had difficulties in sampling the regions at large PI and this precludes extracting reliable information also on the intercalation path. Nonetheless, Figures 3 and 6 point out that the barrier for intercalation is larger for **2**, suggesting that, although the deintercalation paths are energetically similar, the intercalation may disfavor compound **2**, consistently with the fact that this molecule is preferentially an insertor. In order to gain a complete picture of the preferential binding mode of inorganic complexes to DNA, also the insertion mechanisms of these molecules call for further studies.

Due to the increasing interest toward compounds that can target DNA and RNA to act as diagnostic tools, sequence specific probes, or anticancer drugs, our findings can represent a first source of useful information for the design of more effective molecules.[9,18]

dx.doi.org/10.1021/ic5008523 | Inorg. Chem. 2014, 53, 7999−8008

■ ASSOCIATED CONTENT

Supporting Information

Data concerning the estimation of the error on the free energy profiles, test runs for optimization of the path and tables concerning inorganic/complex DNA interaction energy, radial distribution functions and cluster populations, and number of waters wetting the DNA grooves are provided. Figures concerning convergence of the optimization of the path, convergence of metadynamics simulations, the number of waters wetting the MG at the transition state of **2**, and the structures of groove-bound states of both inorganic complexes studied here are also provided. A sketch of different types of intercalators discussed is also shown. This material is available free of charge via the Internet at http://pubs.acs.org.

■ AUTHOR INFORMATION

Corresponding Author

*E-mail: alessandra.magistrato@sissa.it.

Notes

The authors declare no competing financial interest.

■ ACKNOWLEDGMENTS

The authors thank ISCRA Grant HP10CIBWRB for computational resources and the CINECA computing center. Moreover, we thank Dr. D. Branduardi, Dr. G. Bussi, Dr. F. Marinelli, and Dr. F. Pietrucci for useful discussions and suggestions.

■ REFERENCES

(1) Komor, A. C.; Barton, J. K. *Chem. Commun.* **2013**, *49*, 3617.
(2) Erkkila, K. E.; Odom, D. T.; Barton, J. K. *Chem. Rev.* **1999**, *99*, 2777.
(3) Kielkopf, C. L.; Erkkila, K. E.; Hudson, B. P.; Barton, J. K.; Rees, D. C. *Nat. Struct. Biol.* **2000**, *7*, 117.
(4) Zeglis, B. M.; Pierre, V. C.; Barton, J. K. *Chem. Commun.* **2007**, 4565.
(5) Boer, D. R.; Canals, A.; Coll, M. *Dalton Trans* **2009**, 399.
(6) Pierre, V. C.; Kaiser, J. T.; Barton, J. K. *Proc. Natl. Acad. Sci. U.S.A.* **2007**, *104*, 429.
(7) Liu, H. K.; Sadler, P. J. *Acc. Chem. Res.* **2011**, *44*, 349.
(8) Lim, M. H.; Lau, I. H.; Barton, J. K. *Inorg. Chem.* **2007**, *46*, 9528.
(9) Niyazi, H.; Hall, J. P.; O'Sullivan, K.; Winter, G.; Sorensen, T.; Kelly, J. M.; Cardin, C. J. *Nat. Chem.* **2012**, *4*, 621.
(10) Weidmann, A. G.; Komor, A. C.; Barton, J. K. *Philos. Trans. A Math Phys. Eng. Sci.* **2013**, *371*, 20120117.
(11) McConnell, A. J.; Lim, M. H.; Olmon, E. D.; Song, H.; Dervan, E. E.; Barton, J. K. *Inorg. Chem.* **2012**, *51*, 12511.
(12) McKinley, A. W.; Lincoln, P.; Tuite, E. M. *Dalton Trans* **2013**, *42*, 4081.
(13) Bazzicalupi, C.; Biagini, S.; Bianchi, A.; Biver, T.; Boggioni, A.; Giorgi, C.; Gratteri, P.; Malavolti, M.; Secco, F.; Valtancoli, B.; Venturini, M. *Dalton Trans* **2010**, *39*, 9838.
(14) Walker, M. G.; Gonzalez, V.; Chekmeneva, E.; Thomas, J. A. *Angew. Chem., Int. Ed.* **2012**, *51*, 12107.
(15) Zeglis, B. M.; Barton, J. K. *Nat. Protoc.* **2007**, *2*, 357.
(16) Zeglis, B. M.; Boland, J. A.; Barton, J. K. *Biochemistry* **2009**, *48*, 839.
(17) Zeglis, B. M.; Boland, J. A.; Barton, J. K. *J. Am. Chem. Soc.* **2008**, *130*, 7530.
(18) Song, H.; Kaiser, J. T.; Barton, J. K. *Nat. Chem.* **2012**, *4*, 615.
(19) Lim, M. H.; Song, H.; Olmon, E. D.; Dervan, E. E.; Barton, J. K. *Inorg. Chem.* **2009**, *48*, 5392.
(20) Rizzo, V.; Sacchi, N.; Menozzi, M. *Biochemistry* **1989**, *28*, 274.
(21) Chaires, J. B.; Dattagupta, N.; Crothers, D. M. *Biochemistry* **1985**, *24*, 260.
(22) Biver, T.; Secco, F.; Venturini, M. *Coord. Chem. Rev.* **2008**, *252*, 1163.
(23) Biver, T.; Secco, F.; Tine, M. R.; Venturini, M.; Bencini, A.; Bianchi, A.; Giorgi, C. *J. Inorg. Biochem.* **2004**, *98*, 1531.
(24) Biver, T.; Cavazza, C.; Secco, F.; Venturini, M. *J. Inorg. Biochem.* **2007**, *101*, 461.
(25) Mukherjee, A.; Lavery, R.; Bagchi, B.; Hynes, J. T. *J. Am. Chem. Soc.* **2008**, *130*, 9747.
(26) Sasikala, W. D.; Mukherjee, A. *Phys. Chem. Chem. Phys.* **2013**, *15*, 6446.
(27) Sasikala, W. D.; Mukherjee, A. *J. Phys. Chem. B* **2012**, *116*, 12208.
(28) Barducci, A.; Bussi, G.; Parrinello, M. *Phys. Rev. Lett.* **2008**, *100*, 020603.
(29) Branduardi, D.; Gervasio, F. L.; Parrinello, M. *J. Chem. Phys.* **2007**, *126*, 054103.
(30) Limongelli, V.; Bonomi, M.; Marinelli, L.; Gervasio, F. L.; Cavalli, A.; Novellino, E.; Parrinello, M. *Proc. Natl. Acad. Sci. U.S.A.* **2010**, *107*, 5411.
(31) Grazioso, G.; Limongelli, V.; Branduardi, D.; Novellino, E.; De Micheli, C.; Cavalli, A.; Parrinello, M. *J. Am. Chem. Soc.* **2012**, *134*, 453.
(32) Bešker, N.; Gervasio, F. L. *Methods Mol. Biol.* **2012**, *819*, 501.
(33) Favia, A. D.; Masetti, M.; Recanatini, M.; Cavalli, A. *PLoS One* **2011**, *6*, e25375.
(34) Lodola, A.; Branduardi, D.; De Vivo, M.; Capoferri, L.; Mor, M.; Piomelli, D.; Cavalli, A. *PLoS One* **2012**, *7*, e32397.
(35) Hall, J. P.; O'Sullivan, K.; Naseer, A.; Smith, J. A.; Kelly, J. M.; Cardin, C. J. *Proc. Natl. Acad. Sci. U.S.A.* **2011**, *108*, 17610.
(36) Vargiu, A. V.; Magistrato, A. *Inorg. Chem.* **2012**, *51*, 2046.
(37) Hart, J. R.; Glebov, O.; Ernst, R. J.; Kirsch, I. R.; Barton, J. K. *Proc. Natl. Acad. Sci. U.S.A.* **2006**, *103*, 15359.
(38) Orozco, M.; Noy, A.; Perez, A. *Curr. Opin. Struct. Biol.* **2008**, *18*, 185.
(39) Case, D. A.; Cheatham, T. E.; Darden, T.; Gohlke, H.; Luo, R.; Merz, K. M.; Onufriev, A.; Simmerling, C.; Wang, B.; Woods, R. J. *J. Comput. Chem.* **2005**, *26*, 1668.
(40) Robertazzi, A.; Vargiu, A. V.; Magistrato, A.; Ruggerone, P.; Carloni, P.; de Hoog, P.; Reedijk, J. *J. Phys. Chem. B* **2009**, *113*, 10881.
(41) Maurer, P.; Laio, A.; Hugosson, H. W.; Colombo, M. C.; Rothlisberger, U. *J. Chem. Theory Comput.* **2007**, *3*, 628.
(42) Spiegel, K.; Magistrato, A.; Maurer, P.; Ruggerone, P.; Rothlisberger, U.; Carloni, P.; Reedijk, J.; Klein, M. L. *J. Comput. Chem.* **2008**, *29*, 38.
(43) Jorgensen, W.; Chandrasekhar, J.; Madura, J.; Impey, R.; Klein, M. *J. Chem. Phys.* **1983**, *79*, 926.
(44) Aqvist, J. *J. Phys. Chem.* **1990**, *94*, 8021.
(45) Nosè, S. *J. Chem. Phys.* **1984**, *81*, 511.
(46) Van der Spoel, D.; Lindahl, E.; Hess, B.; Groenhof, G.; Mark, A. E.; Berendsen, H. J. C. *J. Comput. Chem.* **2005**, *26*, 1701.
(47) Grubmüller, H.; Heymann, B.; Tavan, P. *Science* **1996**, *271*, 997.
(48) Bonomi, M.; Branduardi, D.; Bussi, G.; Camilloni, C.; Provasi, D.; Raiteri, P.; Donadio, D.; Marinelli, F.; Pietrucci, F.; Broglia, R. A.; Parrinello, M. *Comput. Phys. Commun.* **2009**, *180*, 1961.
(49) Laio, A.; Gervasio, F. L. *Rep. Prog. Phys.* **2008**, *71*, 126601.
(50) Barducci, A.; Bonomi, M.; Parrinello, M. *Wiley Interdisciplinary Reviews: Computational Molecular Science* **2011**, *1*, 826.
(51) Lavery, R.; Sklenar, H. *J. Biomol. Struct. Dyn.* **1989**, *6*, 655.
(52) Lavery, R.; Moakher, M.; Maddocks, J. H.; Petkeviciute, D.; Zakrzewska, K. *Nucleic Acids Res.* **2009**, *37*, 5917.
(53) Humphrey, W.; Dalke, A.; Schulten, K. *J. Mol. Graphics* **1996**, *14*, 33.
(54) Lah, J.; Vesnaver, G. *J. Mol. Biol.* **2004**, *342*, 73.
(55) Vargiu, A. V.; Ruggerone, P.; Magistrato, A.; Carloni, P. *Nucleic Acids Res.* **2008**, *36*, 5910.
(56) Magistrato, A.; Ruggerone, P.; Spiegel, K.; Carloni, P.; Reedijk, J. *J. Phys. Chem. B* **2006**, *110*, 3604.
(57) Spiegel, K.; Magistrato, A.; Carloni, P.; Reedijk, J.; Klein, M. L. *J. Phys. Chem. B* **2007**, *111*, 11873.

(58) Wei, D.; Wilson, W. D.; Neidle, S. *J. Am. Chem. Soc.* **2013**, *135*, 1369.
(59) Haq, I.; Lincoln, P.; Suh, D.; Norden, B.; Chowdry, B.; Chaires, J. *J. Am. Chem. Soc.* **1995**, *117*, 4788.
(60) Starikov, E. B.; Norden, B. *J. Phys. Chem. B* **2007**, *111*, 14431.
(61) Garcia, B.; Ibeas, S.; Ruiz, R.; Leal, J. M.; Biver, T.; Boggioni, A.; Secco, F.; Venturini, M. *J. Phys. Chem. B* **2009**, *113*, 188.
(62) Wilhelm, M.; Mukherjee, A.; Bouvier, B.; Zakrzewska, K.; Hynes, J. T.; Lavery, R. *J. Am. Chem. Soc.* **2012**, *134*, 8588.
(63) Holmlin, R. E.; Stemp, E. D.; Barton, J. K. *Inorg. Chem.* **1998**, *37*, 29.
(64) Holmlin, R. E.; Stemp, E. D. A.; Barton, J. K. *J. Am. Chem. Soc.* **1996**, *118*, 5236.
(65) Neidle, S. *Nat. Chem.* **2012**, *4*, 594.
(66) (Editorial). *Nat. Chem.* **2012**, *4*, 587.
(67) Lewis, E. A.; Munde, M.; Wang, S.; Rettig, M.; Le, V.; Machha, V.; Wilson, W. D. *Nucleic Acids Res.* **2011**, *39*, 9649.
(68) Dolenc, J.; Baron, R.; Oostenbrink, C.; Koller, J.; van Gunsteren, W. F. *Biophys. J.* **2006**, *91*, 1460.
(69) Vargiu, A. V.; Magistrato, A. *ChemMedChem* **2014**, DOI: 10.1002/cmdc.201402203.